Chemosphere 307 (2022) 135680

Contents lists available at ScienceDirect

Chemosphere

journal homepage: www.elsevier.com/locate/chemosphere

Intracellular fate and immune response of porphyrin-based nano-sized metal-organic frameworks

Fang Hao [a,b,d], Zhu-Ying Yan [a], Xiu-Ping Yan [a,b,c,d,*]

[a] State Key Laboratory of Food Science and Technology, Jiangnan University, Wuxi, 214122, China
[b] International Joint Laboratory on Food Safety, Jiangnan University, Wuxi, 214122, China
[c] Key Laboratory of Synthetic and Biological Colloids, Ministry of Education, Jiangnan University, Wuxi, 214122, China
[d] Institute of Analytical Food Safety, School of Food Science and Technology, Jiangnan University, Wuxi, 214122, China

HIGHLIGHTS

- Cellular distribution and endocytosis mechanism of PCN-224 were studied.
- Pathway for immune response of macrophages induced by PCN-224 was elucidated.
- Size-dependent biological effects of PCN-224 under sublethal dose were observed.

GRAPHICAL ABSTRACT

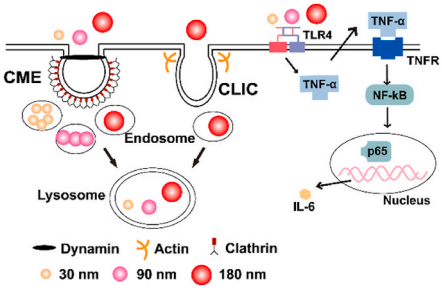

ARTICLE INFO

Handling editor: Willie Peijnenburg

Keywords:
MOFs
Endocytosis pathway
Distribution and localization
Cytokines release

ABSTRACT

The diverse applications of porphyrin-based nano-sized metal-organic frameworks (NMOFs) lead to great exposure risks to human and environment. Understanding the cellular biological effects (such as toxicity, distribution, and localization) of porphyrinic NMOFs is a prerequisite to the assessment of their health risk. However, the characteristics of distribution, localization, and immune response induced by porphyrinic NMOFs have not been studied yet. Here, we report the size-dependent biological effects of porphyrinic NMOFs under sublethal dose. Various sizes of PCN-224 (30, 90, and 180 nm) were taken as model porphyrinic NMOFs. We found that 30 nm PCN-224 gave the highest uptake content, followed by 90 and 180 nm PCN-224. The mechanism for uptake was clathrin-mediated for 30 and 90 nm PCN-224, but clathrin- and glycosylphosphatidylinositol-mediated for 180 nm PCN-224. All PCN-224 were localized in lysosome with size-dependent velocity of colocalization transport. 30 nm PCN-224 induced the highest released cytokines than 90 and 180 nm PCN-224 accompanied with the activation of NF-κB pathway. This work reveals the mechanisms for the endocytosis of PCN-224 and the release of cytokine induced by PCN-224, which is helpful for the health risk assessment of NMOFs.

* Corresponding author. Institute of Analytical Food Safety, School of Food Science and Technology, Jiangnan University, Wuxi, 214122, China.
E-mail address: xpyan@jiangnan.edu.cn (X.-P. Yan).

https://doi.org/10.1016/j.chemosphere.2022.135680
Received 30 May 2022; Received in revised form 8 July 2022; Accepted 9 July 2022
Available online 15 July 2022

1. Introduction

Nano-sized metal-organic frameworks (NMOFs), a class of highly ordered crystalline porous materials (Stock and Biswas, 2012; Kirchon et al., 2018), have been utilized in various areas, especially in environmental protection including heterogenous catalysis and adsorption because of their customized pore size, high surface area and porosity, and intriguing functionality (Horcajada et al., 2012; Cai et al., 2015). Till 2020, over 27 companies are working on the large-scale synthesis and commercialization of MOFs with low cost and high space–time yield (Chen et al., 2021b; Freund et al., 2021). As a result, several NMOF-containing products have been driven to market (2016; Xu and Yaghi, 2020). Despite of the great convenience and high performance of NMOF-containing products, the real-world applications of NMOFs make them release into the environment inevitably, leading to exposure risks for humans and organisms.

Porphyrin-based NMOFs are a subfamily of NMOFs, composed of porphyrin organic linker and metal nodes linked via coordination bonds. The secondary building units (SBU) of metal nodes endow porphyrin-based NMOFs with high chemical stability (Chen et al., 2021a), making them one of the most promising MOF materials in catalysis, molecular adsorption and separation, drug delivery and therapy, and fluorescence sensing (Horcajada et al., 2012; Bai et al., 2016; Islamoglu et al., 2020; Rojas and Horcajada, 2020). The wide application of porphyrin-based NMOFs leads to significant environmental release including the discharge in the manufacture process, fragmentation under physical forces in the usage, and effusion from waste products in the disposal, leading to intentional and accidental exposure risks to humans. Therefore, it is an urgent necessary to comprehensively assess the potential health risks of porphyrin-based NMOFs during their life cycle (Zhang et al., 2021). For this purpose, the study on biological effects including toxicity and distribution is required to fully understand the health risks of porphyrin-based NMOFs before they enter market (Liu et al., 2018).

The intrinsic properties of porphyrin-based NMOFs (such as shape, topology, and dose) have significant effect on their toxicity. The spherical PCN-224 and rod-shape PCN-222 have the same building blocks and similar hydrodynamic sizes, but PCN-222 gave lower percentage of cell necrosis than PCN-224 in the same concentration range (Hao et al., 2022). For different topological structures of porphyrinic NMOFs (PCN-224, MOF-525, PCN-223 and PCN-222) against bacteria, PCN-222 with large pore topology had high ROS generation and cytotoxicity (Liu et al., 2021). Study on the toxicity of four transition metal incorporated aluminum-based porphyrin NMOFs showed that all NMOFs inhibited algal growth and reduced the chlorophyll content due to the release of metal ions and ROS generation (Li et al., 2021b). In addition, 80 nm PCN-224 made significant ROS generation, cytokines release, and cytomembrane damage on RAW264.7 cells accompanied with the activation of autophagy pathway at no less than 20 μg mL^{-1} (Li et al., 2021a). However, the distribution characteristics (*i.e.,* internalization and localization) of porphyrinic NMOFs have not been reported yet.

Nanoparticles with lethal dose induce significant overt toxicity including rupture of membrane, damage of DNA, decline of cell viability and so on, which occurs transitorily in actual exposure (Zhang et al., 2014). While the indirect effects of nanoparticles with sublethal dose would not give significant toxicity but usually disturb the cellular function at molecular level, resulting in persistent biological effects (Wang et al., 2015; Chen et al., 2017). Thus, indirect effects have the potential to pose cumulative health hazards, suggesting that the study of biological effects under sublethal dose is needed to fully evaluate the health risk of nanoparticles.

Immune system is one of the most important defense against foreign pathogens, containing various phagocytes, cytokines, and inflammatory proteins (Schultz and Grieder, 1987; Parkin and Cohen, 2001). Among these phagocytes, macrophages are thought as a vital sentinel cell in combating pathogens and engulfing nanoparticles from circulatory system and organs, making them an ideal model in health risk assessment of NMOFs (Gao et al., 2017; Qu et al., 2017). However, the cellular immune response of macrophages induced by porphyrinic NMOFs is still lack of study.

Herein, we report the intracellular fate and immune response of porphyrinic NMOFs with different sizes. Three kinds of PCN-224 (*i.e.,* 30, 90, and 180 nm PCN-224, structure in Fig. S1) with meso-tetra(4-carboxyphenyl)porphine (TCPP) as the linker to connect the Zr nodes are selected as model porphyrinic NMOFs because they have great opportunity in exposure to humans in the usage of catalysis, sensing and biomedical science. The sublethal dose of PCN-224 was firstly confirmed by viability assay to make basis for further study. The endocytosis kinetics and related mechanism, colocalization characteristics, and the activation of immune response pathway are also demonstrated. Our study improves the understanding of the health risk of porphyrinic NMOFs under sublethal dose, and provides a unique insight into the potential adverse effects of porphyrinic NMOFs on human health.

2. Materials and methods

2.1. Materials

Phosphate buffer saline solution (PBS, pH 7.4) was purchased from Invitrogen (China). Dulbecco's modified Eagle's medium (DMEM) was supplied by Gibco (China). All other reagents were supplied by Aladdin Chemistry Co. Ltd. (China).

2.2. Preparation and characterization of different sizes of PCN-224

PCN-224 (30, 90, and 180 nm) were prepared according to Park et al. (Park et al., 2016). Briefly, 0.22 g benzoic acid (BA) were mixed with 10 mg TCPP and 30 mg $ZrOCl_2{\cdot}8H_2O$ in 10 mL *N,N*-dimethyformamide (DMF) to obtain 30 nm PCN-224. As for the synthesis of 90 and 180 nm PCN-224, the amount of BA were 0.26 g and 0.28 g, respectively. The mixture was heated to 90 °C with stirring for 5 h. The as-prepared PCN-224 was washed for three times with DMF and characterized according to our previous studies (Liu et al., 2021; Hao and Yan, 2022; Hao et al., 2022).

2.3. Cell culture and viability assay

Macrophages (J774A.1) were cultured in DMEM with supplement of 10% fetal bovine serum (FBS, Gibco, USA) and 1 × penicillin-streptomycin (P–S, Invitrogen, USA) at 37 °C and 5% CO_2.

J774A.1 cells were seeded into 96-well plates with the density of 10^4 per well. The cells were then treated with 30, 90, and 180 nm PCN-224 or PBS (negative control) for 24 h, followed by the addition of 10 μM resazurin (MedChemExpress, China) for additional 2 h. The fluorescent intensity at 590 nm (ex. 530 nm) was measured on a multiplate reader (Synergy H1, Biotek, USA).

2.4. Analysis for reactive oxygen species (ROS) and Ca^{2+} flux

J774A.1 cells were incubated with 2,7-dichlorodihydrofluorescein diacetate (DCFH-DA, 10 μM, MedChemExpress) for 1 h and rinsed with PBS for three times. PCN-224 was then added for additional incubation of 2 h, 6 h, and 12 h. The group without PCN-224 treatment was used as negative control. The fluorescent intensity at 530 nm (ex. 485 nm) was measured on a multiplate reader.

Intracellular Ca^{2+} was determined by Fluo/AM probe (Beyotime, China). J774A.1 cells exposed to PCN-224 or PBS (negative control) were incubated with Fluo/AM probe (4 μM) in dark for 20 min and washed with PBS for three times. One aliquot was imaged on an Olympus laser scanning confocal microscopy (LSCM, FV3000) in the range of 500–550 nm under excitation at 488 nm. Another aliquot was

used to obtain the fluorescent intensity of intracellular Ca^{2+} at 530 nm on a multiplate reader under excitation at 485 nm. The relative content of Ca^{2+} was presented as relative fluorescent intensity compared to negative control.

2.5. Endocytosis and exocytosis of PCN-224

J774A.1 cells were seeded on 12-well plates and treated with PBS (negative control) or 5 nM PCN-224 for different periods (2, 6, 12, and 18 h), followed by PBS washing. The harvested cells were lysed with lysis buffer (Solarbio, China) containing 1 × phosphatase/protease inhibitor (Beyotime, China) and digested with regia at 80 °C for 12 h (Hao and Yan, 2022). Then, samples were analyzed for Zr by inductively coupled plasma-mass spectrometry (ICP-MS).

In the exocytosis study, J774A.1 cells were exposed to 5 nM PCN-224 for 6 h and rinsed with PBS at least three times. Then, these cells were cultured in fresh culture medium for additional 6 and 24 h. The medium and cells were digested for ICP-MS determination as mentioned above.

2.6. Endocytosis pathway analysis

Cells were seeded on 12-well plates or confocal dishes with the treatment of different endocytosis inhibitors (MedChemExpress, China), including 55 μM nystatin, 25 μM amiloride, 200 μM methyl-β-cyclodextrin (Me-β-CD), 100 μM chloroquine, and 30 μM 7-ketocholesterol for 1 h. The as-prepared cells were then treated with 5 nM PCN-224 for 6 h and rinsed with PBS (3 times). The cells seeded on 12-well plates were lysed and digested for ICP-MS measurement as mentioned above, while the cells seeded on confocal dishes were fixed in 4% paraformaldehyde (Beyotime, China) and imaged on a LSCM after DAPI (Thermo Fisher, USA) staining. The excitation wavelength was set at 488 nm and emission wavelengths for DAPI and PCN-224 were set at 420–450 nm and 620–700 nm, respectively.

2.7. Fluorescence colocalization staining

J774A.1 cells (10^4 per well) were incubated with PCN-224 (30 nm, 90 nm and 180 nm) at 5 nM for different periods, and followed by PBS washing. Then, the lysosomal probe (100 nM, Lyso-Tracker Green, Beyotime) or mitochondrial probe (50 nM, Mito-Tracker Green, Beyotime) was added for additional 0.5 h incubation. The images were collected on LSCM in the emission range of 500–550 nm and 620–700 nm for probe and PCN-224, respectively, under excitation at 488 nm. The pearson's correlation coefficient (PCC) was calculated by the in-built software Imaris.

2.8. Immunofluorescence staining

J774A.1 cells were fixed with 4% paraformaldehyde after incubation with 5 nM PCN-224 for 6 h. The cells were incubated with blocking buffer (10% goat serum, Solarbio, China) to block non-specific binding sites at room temperature for 1 h. Then, PBS containing 0.1% Triton-X100 was added to the cells for additional 10-min incubation. The as-prepared cells were washed by PBS for 5 min with three replicates and added with anti-phospho–NF–κB antibody (Cell Signaling Technology, USA) with a dilution of 1:200 at 4 °C overnight. The secondary antibody labeled with Alexa-488 (Beyotime, China) was then added with a dilution of 1:1000 for 1 h. The images were collected on a LSCM according to previous studies (Tao et al., 2021; Hao and Yan, 2022).

2.9. Enzyme-linked immunosorbent assay (ELISA)

The released IL-6 and TNF-α from J774A.1 cells were measured with commercial ELISA kits (MULTI SCIENCES, China). The cells were exposed to PCN-224 (0, 1, 2, 5, and 10 nM) for 24 h and the medium was collected for measurement of IL-6 and TNF-α according to the vendor's instruction.

2.10. Statistical analysis

The difference between control and experimental groups was examined by student test. The p values less than 0.05 were set as significant difference. All experiments were repeated for at least three times and represented as mean ± standard deviation.

3. Results and discussion

3.1. Cytotoxicity and cellular response of PCN-224 to macrophages

Prior to the assessment of cytotoxicity, PCN-224 were characterized in the aspect of morphology and photophysical property. Their morphology and solid diameter, fluorescence spectra, UV–vis spectra and hydrodynamic diameter were consistent with those in previous work (Fig. S2 and Table S1) (Hao et al., 2022), suggesting that the synthesis of PCN-224 was successful. Besides, the tested PCN-224 maintained stable in DMEM medium for 24 h (Park et al., 2016; Hao et al., 2022), indicating their dissolution was negligible.

The effect of PCN-224 on viability of J774A.1 cells, a well-known macrophage model, was employed to evaluate the effect of PCN-224 on cell viability. In general, all the studied PCN-224 made cell viability increase with the concentration of PCN-224 no more than 5 nM, then decrease with further increase of the concentration of PCN-224 to 20 nM (Fig. 1A). The studied PCN-224 exhibited size-dependent cytotoxicity, *i.e.,* larger sized PCN-224 gave less cytotoxicity. The increasing cell viability with the exposure to nanoparticles was also reported by other studies mainly due to the effect of stress for nanoparticles (RuyraÀ. Yazdi et al., 2015; Chen et al., 2020; Yan et al., 2021). Fig. 1A also shows that PCN-224 with concentration less than 10 nM gave more than 80% viability of J774A.1 cells, suggesting this concentration had no overt toxic effect on cells.

The intracellular ROS generation of PCN-224 was evaluated using a turn-on fluorescent probe (DCFH-DA). Excessive ROS generation is an important cellular response in the exposure of cells to nanoparticles as ROS is an important signal molecule in inflammation reaction, cytokines secretion and so on (Aranda et al., 2013; Tao et al., 2021). Fig. 1B shows the relative content of ROS had no significant change in 5 nM PCN-224-treated groups compared to negative control, indicating PCN-224 with the concentration of 5 nM had no effect on intracellular ROS equilibrium.

Accumulation of Ca^{2+} flux is an early and sensitive indicator in cellular response as it is usually associated with mitochondrial dysfunction, cytoskeletal rearrangement, and inflammation (Bagur and Hajnóczky, 2017; Gao et al., 2017; Wang et al., 2021). Therefore, we investigated the effect of PCN-224 on the Ca^{2+} flux of J774A.1 cells using a turn-on fluorescent probe. The relative contents of Ca^{2+} in 30, 90, and 180 nm PCN-224 treated cells show no difference compared to control group (without PCN-224 treatment) (Fig. 1C and Fig. S3), suggesting the PCN-224 could not induce the accumulation of Ca^{2+} flux in the concentration range of 1–5 nM. This was also confirmed by the LSCM images in Fig. 1D.

In summary, the exposure of 30, 90, and 180 nm PCN-224 to J774A.1 cells had no adverse effect on cellular response with the concentration from 1 to 5 nM. Therefore, 5 nM was adopted as the sublethal dose for the following studies to evaluate the distribution and immune response of PCN-224.

3.2. Cellular endocytosis and exocytosis of PCN-224

Endocytosis and exocytosis are critical steps in evaluating the intracellular distribution of nanoparticles. Understanding the kinetics of the endocytosis of PCN-224 could accurately document the internalization process. The intracellular content of PCN-224 (as Zr) per million

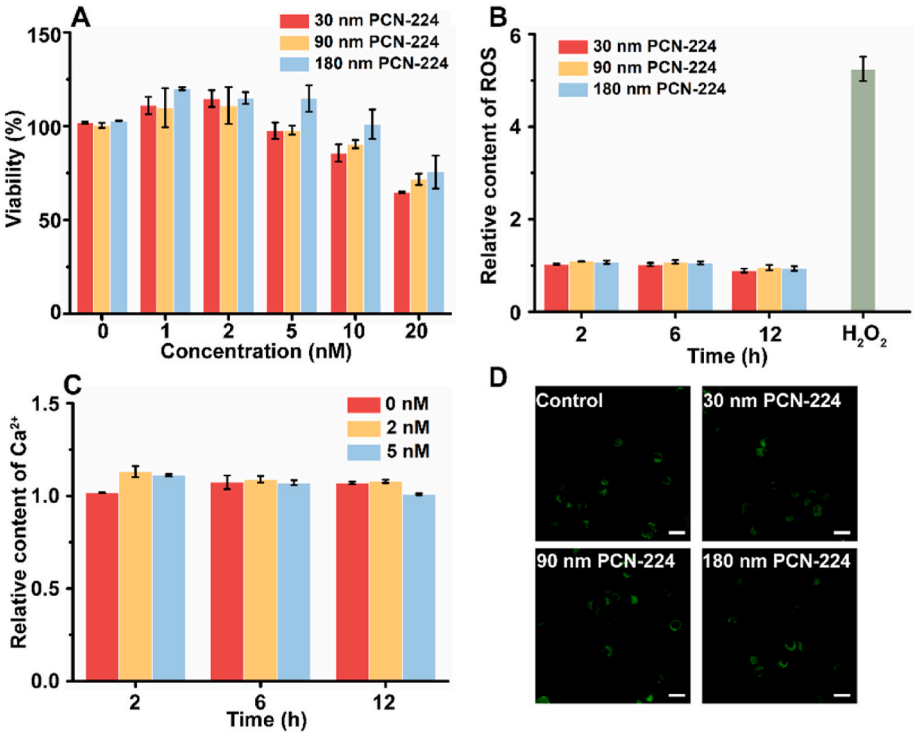

Fig. 1. (A) Cell viability of J774A.1 after incubation with various concentrations of PCN-224 for 24 h. (B) ROS generation in J774A.1 cells exposed to PCN-224 (5 nM) compared to PBS-treated cells (negative control) for different periods. 10 mM H_2O_2 was set as positive control. (C) Relative content of Ca^{2+} in J774A.1 cells incubated with 30 nm PCN-224. (D) Fluorescence images of Ca^{2+} in J774A.1 cells treated with 5 nM PCN-224 for 6 h. Scale bars 20 μm.

cells was measured on an ICP-MS (Fig. 2A). The uptake kinetic curves show the intracellular content of 30, 90, and 180 nm PCN-224 reached 54.8, 39.9, and 32.4 μg per million cells after 6 h incubation, respectively, then elevated slowly from 6 to 18 h, indicating the cellular uptake of PCN-224 reached almost saturation in the first 6 h. The content of PCN-224 per million cells decreased as the size of PCN-224 increased.

The exocytosis of 30, 90, and 180 nm PCN-224 was studied by ICP-MS. Exocytosis is a detoxifying process for cells through active transportation to decrease the internalized nanoparticles, resulting in different cellular distribution of nanoparticles (Bourquin et al., 2019; Ku et al., 2021). Fig. 2B shows a small proportion of PCN-224 (0.6%–1.7%) was excreted from macrophages after incubation for 6–24 h, but the relative contents of all intracellular PCN-224 were still more than 98%, suggesting the exocytosis for all the studied sizes of PCN-224 was negligible. Previous studies also confirmed that cancer cells could reduce the intracellular nanoparticles through the cell division instead of exocytosis both in 2D culture and in 3D culture, suggesting the endocytosis of nanoparticles is irreversible (Mazuel et al., 2016; Bourquin et al., 2019).

3.3. Mechanism for the endocytosis of PCN-224

The endocytosis pathway for PCN-224 was studied with the chemical endocytosis inhibitors. The mechanism for endocytosis could be divided into five routes: caveolae-mediated endocytosis, macropinocytosis, lipid raft endocytosis, clathrin-mediated endocytosis (CME), and clathrin-independent carrier/glycosylphosphatidylinositol-anchored protein enriched early endocytic compartment (CLIC/GEEC) endocytosis (Rennick et al., 2021; Sousa de Almeida et al., 2021). To determine which route was responsible for the entrance of PCN-224 into the cells, various chemical endocytosis inhibitors including nystatin, amiloride, Me-β-CD, chloroquine, and 7-ketocholesterol, which could specifically block the

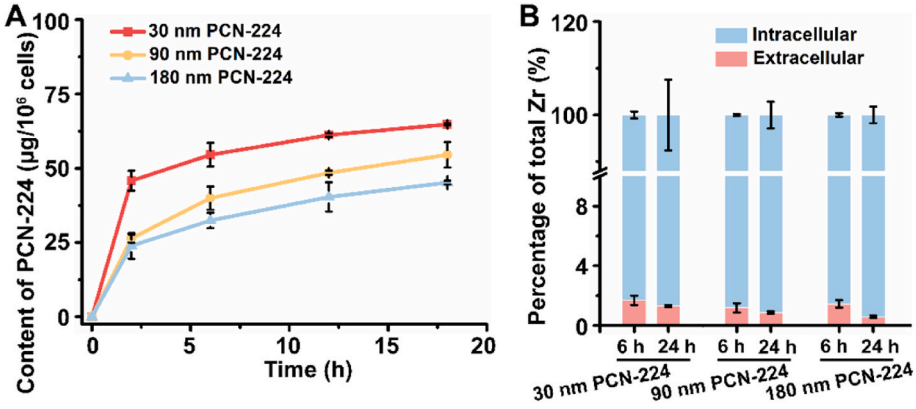

Fig. 2. (A) Cellular uptake of different sizes of PCN-224 (as Zr) at various time intervals. (B) Relative content of extracellular and intracellular PCN-224 (as Zr) at different incubation times. Exposure concentration of PCN-224, 5 nM.

caveolae-mediated endocytosis, macropinocytosis, lipid raft endocytosis, CME, and CLIC/GEEC, respectively, were used. All these inhibitors were nontoxic to J774A.1 cells as revealed by viability assay (Fig. S4). The preincubation of J774A.1 cells with nystatin, amiloride, methyl--β-cyclodextrin (Me-β-CD), and 7-ketocholesterol did not significantly change the uptake of 30 and 90 nm PCN-224 (as Zr) (Fig. 3A). However, chloroquine blocked 40.5% and 48.8% cellular uptake of 30 nm PCN-224 and 90 nm PCN-224, respectively, suggesting the uptake of these two sizes of PCN-224 was through CME pathway. Chloroquine and 7-ketocholesterol inhibited 49.3% and 27.5% of the uptake of 180 nm PCN-224, respectively. The decreased relative uptake of 180 nm PCN-224 indicates that CME and CLIC/GEEC endocytosis contributed to the internalization of 180 nm PCN-224. The internalization of ZIF-8 and ZIF-67 by algal cells was also mediated by multi-pathways while the metal nanoparticles were usually internalized through one pathway (Zhang et al., 2014; Zhang et al., 2021; Li et al., 2022). Therefore, the NMOF may give a distinct internalization pattern. The mechanism of endocytosis was also confirmed by fluorescence staining. Fig. 3B shows the nucleus (blue) stained with DAPI were surrounded by PCN-224 (red). The red fluorescence intensities of PCN-224 decreased dramatically from 100% to 18%–32% (Fig. S5) after preincubation with chloroquine for 1 h, giving similar decreased patterns in Fig. 3A. The result of internalization suggests that the size of PCN-224 determined the pathway of cellular internalization (Fig. 3C).

3.4. Intracellular distribution of PCN-224

Endocytosis could lead to lysosomal or mitochondrial distribution of nanoparticles, making compromise in autophagy and aerobic metabolism. For instance, MIL-101 in lysosome increased the autophagy flux of 3T3/L1 cells without significant cell toxicity (Shen et al., 2018). The interaction of AgNP and mitochondria induced great ROS generation and loss of mitochondrial potential at sublethal concentrations (Wang et al., 2022). Therefore, clarifying the intracellular distribution of PCN-224 is significant for understanding the potential risks for cells. The subcellular distribution of 30, 90, and 180 nm PCN-224 after internalization was elucidated by fluorescence imaging with counterstaining of lysosome and mitochondria. Fig. 4A shows the red fluorescence of PCN-224 was colocalized partially with green fluorescence of lysosome after 4 h incubation. However, the green fluorescence of lysosome was totally covered by the red fluorescence of PCN-224 after 24 h incubation.

The relative level of colocalization between PCN-224 and lysosome was then evaluated by the Pearson's correlation coefficients (PCC, higher PCC means stronger colocalization). The PCC values of lysosome with 30 nm PCN-224, 90 nm PCN-224, and 180 nm PCN-224 were 0.11, 0.21, and 0.23 after 4 h incubation, respectively, then increased to 0.55, 0.46, and 0.43 after 24 h incubation, respectively (Fig. 4B), indicating that the level of colocalization of PCN-224 and lysosome followed an increasing order of 180 nm PCN-222 < 90 nm PCN-224 < 30 nm PCN-224, in good agreement with the fact that small nanoparticles had fast intracellular transport (Aoyama et al., 2017). However, the colocalization of mitochondria (green) and PCN-224 (red) was negligible (negative PCC values) after 24 h incubation (Fig. S6). The colocalization results indicate that PCN-224 was mostly located in lysosome and the size of PCN-224 determined the velocity of colocalization transport.

3.5. Immune response to PCN-224 exposure

Interleukin 6 (IL-6) and tumor necrosis factor alpha (TNF-α), the two kinds of potent pleiotropic cytokine regulating immune response secreted by macrophages, were then assessed using an ELISA assay to confirm if the exposure of PCN-224 to macrophages under sublethal dose could induce their immune response. The concentration of IL-6 (calibration curve in Fig. S7) in PCN-224 treated cells increased with the concentration of PCN-224 (Fig. 5A). 30 nm PCN-224, 90 nm PCN-224, and 180 nm PCN-224 with the concentration of 0–10 nM gave the IL-6 concentration of 8.1–16.5 pg mL^{-1}, 9.2–12.1 pg mL^{-1}, and 8.7–11.0 pg mL^{-1}, respectively. The pattern for the change of the concentration of TNF-α (calibration curve in Fig. S7) was similar to that of IL-6 (Fig. 5B). 30 nm PCN-224, 90 nm PCN-224, and 180 nm PCN-224 with the concentration of 0–10 nM made the concentration of TNF-α increase from 34.0 to 52.5 pg mL^{-1}, 32.0–44.6 pg mL^{-1}, and 30.2–38.1 pg mL^{-1}, respectively. All kinds of PCN-224 made size-dependent increase in the secretion of IL-6 and TNF-α, that is, the smaller in the size of PCN-224, the higher immune response induced.

The release of IL-6 was regulated by the tandem activation of NF-κB pathway (Tao et al., 2021). The NF-κB complex was composed of IκBα, p65, and p50, retaining in cytoplasm (Baldwin, 1996). The activation of NF-κB complex leads to the phosphorylation and degradation of IκBα, and the phosphorylation of p65 with translocation to nucleus (Napetschnig and Wu, 2013). The phosphorylated p65 then regulates the production of IL-6 (Zhou et al., 2012). Therefore, the phosphorylated p65 was detected using the immunofluorescence staining to confirm the activation of NF-κB pathway in J774A.1 cells after incubation with PCN-224. The J774A.1 cells exposed to PCN-224 gave stronger fluorescence than control cells, indicating the occurrence of phosphorylation of p65 (Fig. 5C). Besides, 30 nm PCN-224 made green fluorescence

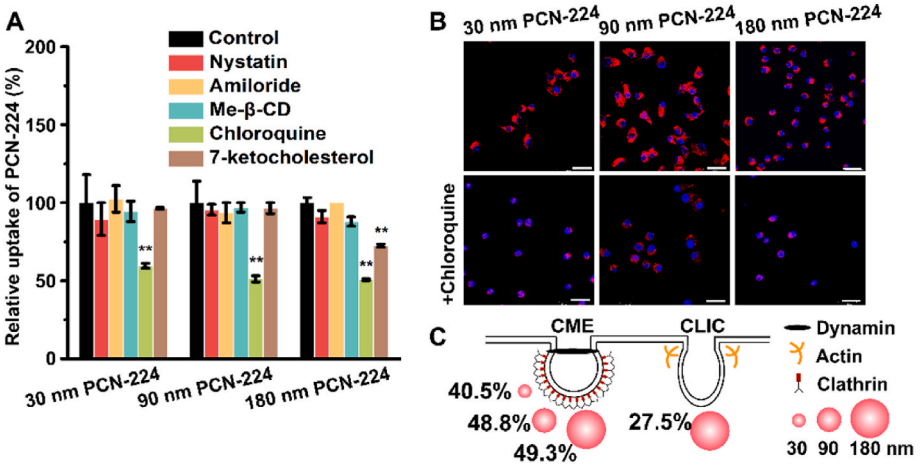

Fig. 3. (A) Relative uptaken content of PCN-224 by J774A.1 cells treated with PBS (control) or inhibitors (Nystatin, 55 μM; amiloride, 25 μM; Me-β-CD, 200 μM; chloroquine, 100 μM; 7-ketocholesterol, 30 μM). Concentration of PCN-224, 5 nM $^{**}p < 0.01$. (B) Fluorescent images of J774A.1 cells exposed to 30 nm, 90 nm, and 180 nm PCN-224 (5 nM) after preincubation with chloroquine (100 μM) for 1 h. (C) Schematic for the uptake pathway of 30, 90 and 180 nm PCN-224.

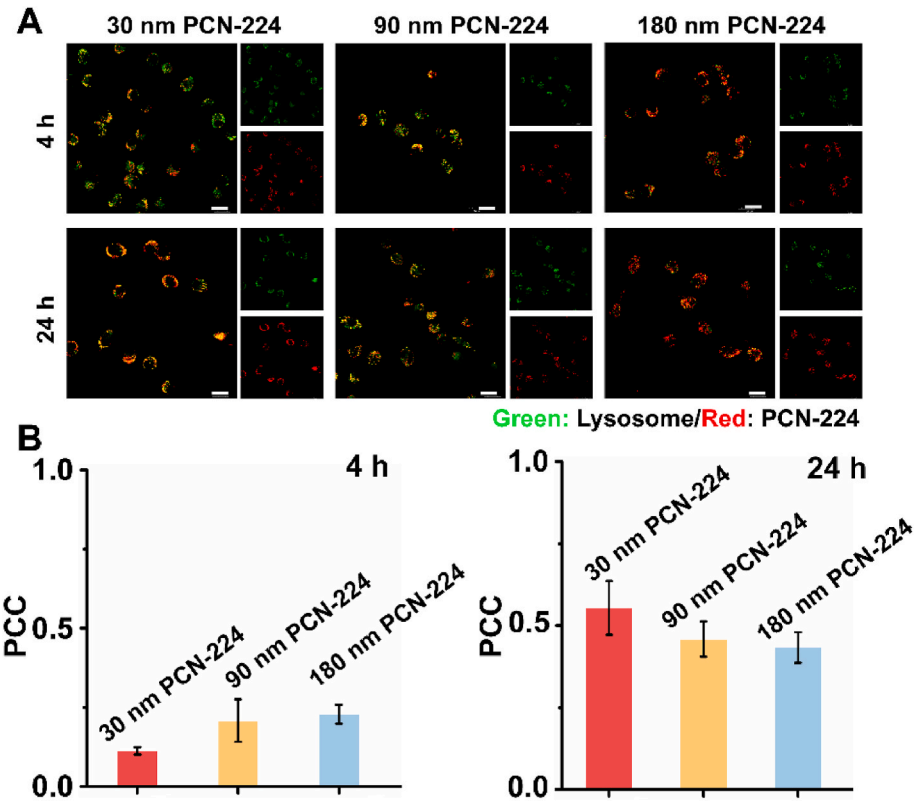

Fig. 4. (A) Subcellular distribution of PCN-224 in J774A.1 cells after 4 and 24 h incubation. Green: lysosome and red: PCN-224. (B) PCC values for the colocalization of PCN-224 and lysosome. Scale bars 20 μm. (For interpretation of the references to colour in this figure legend, the reader is referred to the Web version of this article.)

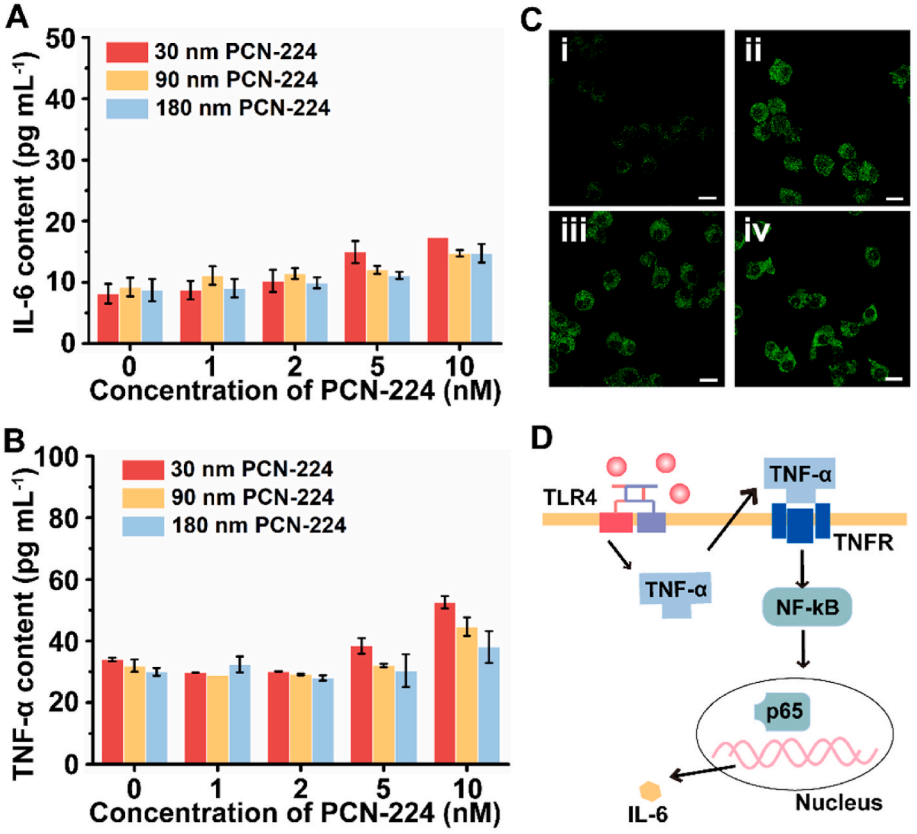

Fig. 5. Concentration of IL-6 protein (A) and TNF-α protein (B) in culture medium secreted from J774A.1 cells after incubation with various concentrations of PCN-224 for 24 h. (C) Immunofluorescence images of phosphorylated NF-κB in J774A.1 cells after incubation with various solutions: (i) PBS (negative control), (ii) 30 nm PCN-224 (5 nM), (iii) 90 nm PCN-224 (5 nM), and (iv) 180 nm PCN-224 (5 nM). Scale bars, 20 μm. (D) Schematic for the mechanisms responsible for PCN-224 induced immune response to J774A.1 cells.

emit from the nucleus of the J774A.1 cells, indicating that phosphorylated p65 translocated from cytoplasm to nucleus. In contrast, 90 and 180 nm PCN-224 treated cells gave lower fluorescence intensity in nucleus than 30 nm PCN-224 treated cells, in good agreement with the pattern for the change of IL-6 concentration (Fig. 5A). The above results suggest the important role of the size of PCN-224 in the activation of NF-κB pathway.

In view of two facts that interaction between nanoparticle and Toll-like receptor (TLR) induces TNF-α production and the TNF-α induced the activation of NF-κB (Zhou et al., 2012; Qu et al., 2013), the autocrine loop of TNF-α drived the release of IL-6 from macrophages (Fig. 5D).

4. Conclusion

In summary, we have reported the cellular distribution, endocytosis, and immune response of different sizes of PCN-224 to J774A.1 cells under sublethal dose. Smaller size of PCN-224 was found to induce higher endocytosis content. Only CME was responsible for the endocytosis of 30 and 90 nm PCN-224, while both CME and CLIC/GEEC were responsible for 180 nm PCN-224. All the studied PCN-224 were located in lysosome after endocytosis and smaller size of PCN-224 exhibited higher colocalization velocity. PCN-224 induced size-dependent release of immune cytokine through the activation of NF-κB pathway, following the increasing order of 180 nm PCN-224 < 90 nm PCN-224 < 30 nm PCN-224. The findings herein not only reveal the cellular fate and related mechanism of nanosized PCN-224, but also deep the understanding of health risks of NMOFs under sublethal dose.

Credit author statement

Hao Fang: Conceptualization, Methodology, Writing- Original draft preparation. Yan Zhu-Ying: Methodology. Yan Xiu-Ping: Supervision, Project administration, Writing- Reviewing and Editing, Funding acquisition.

Declaration of competing interest

The authors declare that they have no known competing financial interests or personal relationships that could have appeared to influence the work reported in this paper.

Data availability

The data that has been used is confidential.

Acknowledgements

This work was supported by the China Postdoctoral Science Foundation (2021M700056), Jiangsu Postdoctoral Research Funding Program (2021K540C), National First-class Discipline Program of Food Science and Technology (JUFSTR20180301), National Natural Science Foundation of China (22176073), State Key Laboratory of Environmental Chemistry and Ecotoxicology, Research Center for Eco-Environmental Sciences, Chinese Academy of Sciences (KF2021-09), and the Program of "Collaborative Innovation Center of Food Safety and Quality Control in Jiangsu Province".

Appendix A. Supplementary data

Supplementary data to this article can be found online at https://doi.org/10.1016/j.chemosphere.2022.135680.

References

Aoyama, M., Yoshioka, Y., Arai, Y., Hirai, H., Ishimoto, R., Nagano, K., Higashisaka, K., Nagai, T., Tsutsumi, Y., 2017. Intracellular trafficking of particles inside endosomal vesicles is regulated by particle size. J. Contr. Release 260, 183–193.
Aranda, A., Sequedo, L., Tolosa, L., Quintas, G., Burello, E., Castell, J.V., Gombau, L., 2013. Dichloro-dihydro-fluorescein diacetate (DCFH-DA) assay: a quantitative method for oxidative stress assessment of nanoparticle-treated cells. Toxicol. Vitro 27, 954–963.
Bagur, R., Hajnóczky, G., 2017. Intracellular Ca^{2+} sensing: its role in calcium homeostasis and signaling. Mol. Cell 66, 780–788.
Bai, Y., Dou, Y., Xie, L.-H., Rutledge, W., Li, J.-R., Zhou, H.-C., 2016. Zr-based metal–organic frameworks: design, synthesis, structure, and applications. Chem. Soc. Rev. 45, 2327–2367.
Baldwin Jr., A.S., 1996. The NF-kappa B and I kappa B proteins: new discoveries and insights. Annu. Rev. Immunol. 14, 649–683.
Bourquin, J., Septiadi, D., Vanhecke, D., Balog, S., Steinmetz, L., Spuch-Calvar, M., Taladriz-Blanco, P., Petri-Fink, A., Rothen-Rutishauser, B., 2019. Reduction of nanoparticle load in cells by mitosis but not exocytosis. ACS Nano 13, 7759–7770.
Cai, W., Chu, C.-C., Liu, G., Wáng, Y.-X.J., 2015. Metal–organic framework-based nanomedicine platforms for drug delivery and molecular imaging. Small 11, 4806–4822.
Chen, Y., Xu, M., Zhang, J., Ma, J., Gao, M., Zhang, Z., Xu, Y., Liu, S., 2017. Genome-wide DNA methylation variations upon exposure to engineered nanomaterials and their implications in nanosafety assessment. Adv. Mater. 29, 1604580.
Chen, P., He, M., Chen, B., Hu, B., 2020. Size- and dose-dependent cytotoxicity of ZIF-8 based on single cell analysis. Ecotoxicol. Environ. Saf. 205, 111110.
Chen, J., Zhu, Y., Kaskel, S., 2021a. Porphyrin-based metal–organic frameworks for biomedical applications. Angew. Chem. Int. Ed. 60, 5010–5035.
Chen, Z., Wasson, M.C., Drout, R.J., Robison, L., Idrees, K.B., Knapp, J.G., Son, F.A., Zhang, X., Hierse, W., Kühn, C., Marx, S., Hernandez, B., Farha, O.K., 2021b. The state of the field: from inception to commercialization of metal–organic frameworks. Faraday Discuss 225, 9–69.
Freund, R., Zaremba, O., Arnauts, G., Ameloot, R., Skorupskii, G., Dincă, M., Bavykina, A., Gascon, J., Ejsmont, A., Gościańska, J., Kalmutzki, M., Lächelt, U., Ploetz, E., Diercks, C., Wuttke, S., 2021. The current status of MOF and COF applications. Angew. Chem. Int. Ed. 60, 23975.
Gao, J., Li, R., Wang, F., Liu, X., Zhang, J., Hu, L., Shi, J., He, B., Zhou, Q., Song, M., Zhang, B., Qu, G., Liu, S., Jiang, G., 2017. Determining the cytotoxicity of rare earth element nanoparticles in macrophages and the involvement of membrane damage. Environ. Sci. Technol. 51, 13938–13948.
Hao, F., Yan, X.-P., 2022. Nano-sized zeolite-like metal-organic frameworks induced hematological effects on red blood cell. J. Hazard Mater. 424, 127353.
Hao, F., Yan, Z.-Y., Yan, X.-P., 2022. Size- and shape-dependent cytotoxicity of nano-sized Zr-based porphyrinic metal-organic frameworks to macrophages. Sci. Total Environ. 833, 155309.
Horcajada, P., Gref, R., Baati, T., Allan, P.K., Maurin, G., Couvreur, P., Férey, G., Morris, R.E., Serre, C., 2012. Metal–organic frameworks in biomedicine. Chem. Rev. 112, 1232–1268.
Islamoglu, T., Chen, Z., Wasson, M.C., Buru, C.T., Kirlikovali, K.O., Afrin, U., Mian, M.R., Farha, O.K., 2020. Metal–organic frameworks against toxic chemicals. Chem. Rev. 120, 8130–8160.
Kirchon, A., Feng, L., Drake, H.F., Joseph, E.A., Zhou, H.-C., 2018. From fundamentals to applications: a toolbox for robust and multifunctional MOF materials. Chem. Soc. Rev. 47, 8611–8638.
Ku, T., Hao, F., Yang, X., Rao, Z., Liu, Q.S., Sang, N., Faiola, F., Zhou, Q., Jiang, G., 2021. Graphene quantum dots disrupt embryonic stem cell differentiation by interfering with the methylation level of Sox2. Environ. Sci. Technol. 55, 3144–3155.
Li, X., Qin, H., Zhou, Z., Li, Y., Wang, J., Lin, M., Dong, X., Yang, M., Li, L., 2021a. Cellular evaluation of the metal-organic framework PCN-224 associated with inflammation and autophagy. Toxicol. Vitro 70, 105019.
Li, Y., Shang, S., Shang, J., Wang, W.-X., 2021b. Toxicity assessment and underlying mechanisms of multiple metal organic frameworks using the green algae Chlamydomonas reinhardtii model. Environ. Pollut. 291, 118199.
Li, D., Zhou, Q., Hu, X., Mu, L., Zeng, H., Luo, J., 2022. Environmental decomposition and remodeled phytotoxicity of framework-based nanomaterials. J. Hazard Mater. 422, 126846.
Liu, S., Lu, Y., Chen, W., 2018. Bridge knowledge gaps in environmental health and safety for sustainable development of nano-industries. Nano Today 23, 11–15.
Liu, Y.-Y., Chen, L.-J., Zhao, X., Yan, X.-P., 2021. Effect of topology on photodynamic sterilization of porphyrinic metal-organic frameworks. Chem. Eur J. 27, 10151–10159.
Mazuel, F., Espinosa, A., Luciani, N., Reffay, M., Le Borgne, R., Motte, L., Desboeufs, K., Michel, A., Pellegrino, T., Lalatonne, Y., Wilhelm, C., 2016. Massive intracellular biodegradation of iron oxide nanoparticles evidenced magnetically at single-endosome and tissue levels. ACS Nano 10, 7627–7638.
Napetschnig, J., Wu, H., 2013. Molecular basis of NF-κB signaling. Annu. Rev. Biophys. 42, 443–468.
Park, J., Jiang, Q., Feng, D., Mao, L., Zhou, H.-C., 2016. Size-controlled synthesis of porphyrinic metal–organic framework and functionalization for targeted photodynamic therapy. J. Am. Chem. Soc. 138, 3518–3525.
Parkin, J., Cohen, B., 2001. An overview of the immune system. Lancet 357, 1777–1789.
Qu, G., Liu, S., Zhang, S., Wang, L., Wang, X., Sun, B., Yin, N., Gao, X., Xia, T., Chen, J.-J., Jiang, G.-B., 2013. Graphene oxide induces toll-like receptor 4 (TLR4)-dependent necrosis in macrophages. ACS Nano 7, 5732–5745.

Qu, G., Liu, W., Zhao, Y., Gao, J., Xia, T., Shi, J., Hu, L., Zhou, W., Gao, J., Wang, H., Luo, Q., Zhou, Q., Liu, S., Yu, X.-F., Jiang, G., 2017. Improved biocompatibility of black phosphorus nanosheets by chemical modification. Angew. Chem. Int. Ed. 56, 14488–14493.

Rennick, J.J., Johnston, A.P.R., Parton, R.G., 2021. Key principles and methods for studying the endocytosis of biological and nanoparticle therapeutics. Nat. Nanotechnol. 16, 266–276.

Rojas, S., Horcajada, P., 2020. Metal–organic frameworks for the removal of emerging organic contaminants in water. Chem. Rev. 120, 8378–8415.

Ruyra, À., Yazdi, A., Espín, J., Carné-Sánchez, A., Roher, N., Lorenzo, J., Imaz, I., Maspoch, D., 2015. Synthesis, culture medium stability, and in vitro and in vivo zebrafish embryo toxicity of metal–organic framework nanoparticles. Chem. Eur J. 21, 2508–2518.

Schultz, K.T., Grieder, F., 1987. Structure and function of the immune system. Toxicol. Pathol. 15, 262–264.

Shen, S., Li, L., Li, S., Bai, Y., Liu, H., 2018. Metal–organic frameworks induce autophagy in mouse embryonic fibroblast cells. Nanoscale 10, 18161–18168.

Sousa de Almeida, M., Susnik, E., Drasler, B., Taladriz-Blanco, P., Petri-Fink, A., Rothen-Rutishauser, B., 2021. Understanding nanoparticle endocytosis to improve targeting strategies in nanomedicine. Chem. Soc. Rev. 50, 5397–5434.

Stock, N., Biswas, S., 2012. Synthesis of metal-organic frameworks (MOFs): routes to various MOF topologies, morphologies, and composites. Chem. Rev. 112, 933–969.

Tao, X., Wan, X., Wu, D., Song, E., Song, Y., 2021. A tandem activation of NLRP3 inflammasome induced by copper oxide nanoparticles and dissolved copper ion in J774A.1 macrophage. J. Hazard Mater. 411, 125134.

Wang, Z., Xia, T., Liu, S., 2015. Mechanisms of nanosilver-induced toxicological effects: more attention should be paid to its sublethal effects. Nanoscale 7, 7470–7481.

Wang, N., Yin, J., You, N., Yang, S., Guo, D., Zhao, Y., Ru, Y., Liu, X., Cheng, H., Ren, Q., Cheng, T., Ma, X., 2021. TWIST1 preserves hematopoietic stem cell function via the CACNA1B/Ca^{2+}/mitochondria axis. Blood 137, 2907–2919.

Wang, F., Chen, Z., Wang, Y., Ma, C., Bi, L., Song, M., Jiang, G., 2022. Silver nanoparticles induce apoptosis in HepG2 cells through particle-specific effects on mitochondria. Environ. Sci. Technol. 56, 5706–5713.

Xu, W., Yaghi, O.M., 2020. Metal–organic frameworks for water harvesting from air, anywhere, anytime. ACS Cent. Sci. 6, 1348–1354.

Yan, X., Yang, Q., Fang, X., Xiong, P., Liu, S., Cao, Z.-Y., Liao, C., Liu, S., Jiang, G., 2021. Co(II)-based metal–organic framework induced apoptosis through kindling the HIF-1α/BNIP3 signaling pathway in microglial cells. Environ. Sci.: Nano 8, 2866–2882.

Zhang, Y., Bai, Y., Jia, J., Gao, N., Li, Y., Zhang, R., Jiang, G., Yan, B., 2014. Perturbation of physiological systems by nanoparticles. Chem. Soc. Rev. 43, 3762–3809.

Zhang, X., Hu, X., Wu, H., Mu, L., 2021. Persistence and recovery of ZIF-8 and ZIF-67 phytotoxicity. Environ. Sci. Technol. 55, 15301–15312.

Zhou, H., Zhao, K., Li, W., Yang, N., Liu, Y., Chen, C., Wei, T., 2012. The interactions between pristine graphene and macrophages and the production of cytokines/chemokines via TLR- and NF-κB-related signaling pathways. Biomaterials 33, 6933–6942.